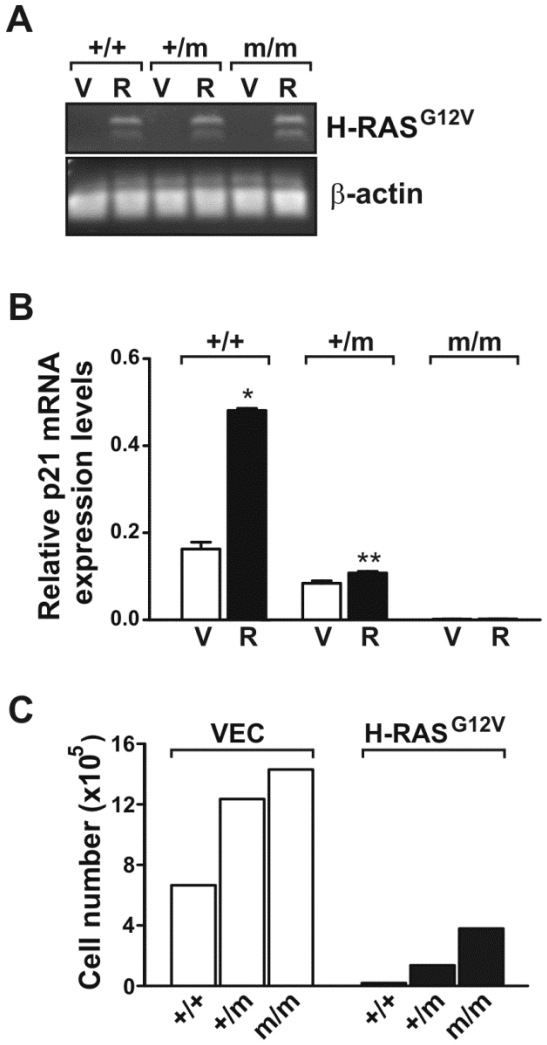

Figure S1. Impaired anti-proliferative effects of mutant H-RAS in pig fibroblasts expressing the porcine p53-R167H mutant protein. Pig fibroblasts expressing wild-type p53 (+/+), one mutant allele of R167H (+/m) or two R167H p53 alleles (m/m) were infected with pBabe-puro vector or pBabe-H-RAS-G12V-puro viruses and selected with puromycin for 7 to 10 days. A) Semi-quantitative RT-PCR analyses demonstrate H-RAS-G12V mRNA expression in Ras-infected (R) but not vector-infected (V) cells. B) Quantitative RT-PCR analyses show that H-RAS-G12V induces p21 mRNA expression in p53 wild-type cells (+/+) relative to vector-infected cells, but has a minimal effect on p21 transcript levels in +/m fibroblasts and no effect in m/m cells. Error bars represent the standard deviation from the mean for triplicate samples with statistical significance calculated using an unpaired, two-tailed Student's t-test (*, $p<0.01$; **, $p<0.05$). C) Cell counts from a representative experiment show that H-RAS-G12V greatly inhibits the proliferation of p53 wild-type cells (~35-fold) relative to vector (VEC) infected control cells but has a modest effect in p53-R167H expressing m/m cells (<4-fold decrease in cell number). These data are consistent with the reduced ability or failure of mutant H-RAS to induce senescence in p53-R167H positive +/m and m/m cells, respectively (Figure 2).

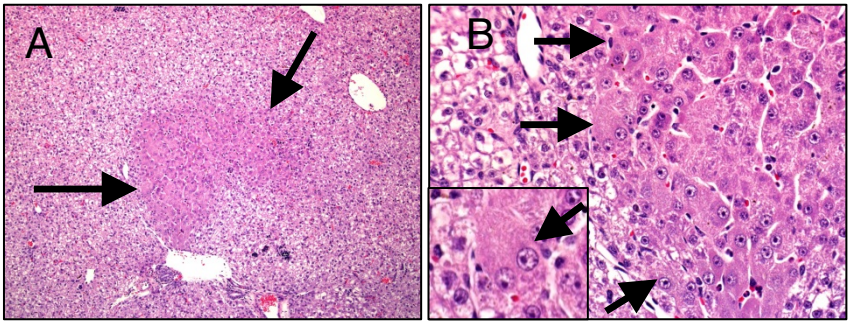

Figure S2. Liver from a neonatal *TP53*$^{R167H/R167H}$ pig, Case 1. A,B) Within the liver, focal atypia (arrows) was composed of irregular hepatic cords with enlarged hepatocellular cells and nuclei, 100 and 400x. Inset: A binucleate hepatocyte (arrow) with marginated chromatin and a prominent nucleolus was much larger than adjacent hepatocytes (lower left, inset).

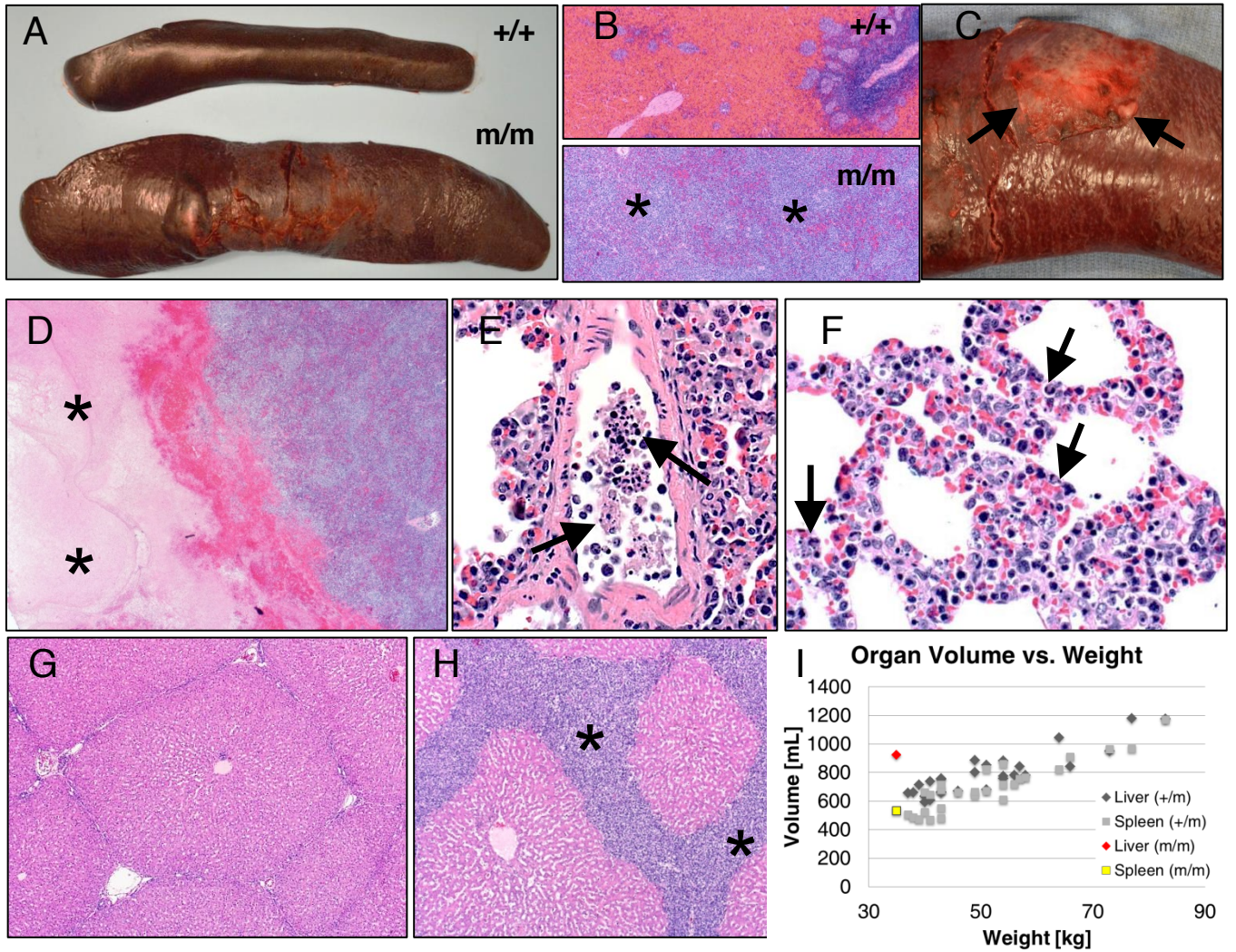

Figure S3. Lymphoma in *TP53*$^{R167H/R167H}$ pigs (m/m). A) Splenomegaly was a consistent finding (bottom, Case 3). B) Spleens were effaced by neoplastic lymphocytes (asterisks, bottom panel, Case 3), 40x. C) In Case 2, the spleen had ruptured with fibrinous exudate on the surface of the capsule (arrows). D) Microscopically, the ruptured spleen (Case 2) had necrotic foci (asterisks) and hemorrhage (red color, 20x). E,F) The lung in Case 2 had intravascular emboli composed of cellular and nuclear debris with neoplastic cells occluding numerous arteries (arrows, E, 400x) and capillaries in alveolar septa (arrows, F, 400x) - consistent with tumor lysis syndrome. G,H) Lymphoma pigs often had bridging infiltration by lymphoma cells (asterisks) in portal regions of the liver (right panel, Case 4), 40x. I) Trends for liver and spleen volumes as segmented from CT, relative to animal weight for a cohort of *TP53*$^{R167H/+}$ pigs, showing the significantly elevated liver volume for lymphoma Case 4 (red diamond) and slightly elevated spleen volume (yellow square).

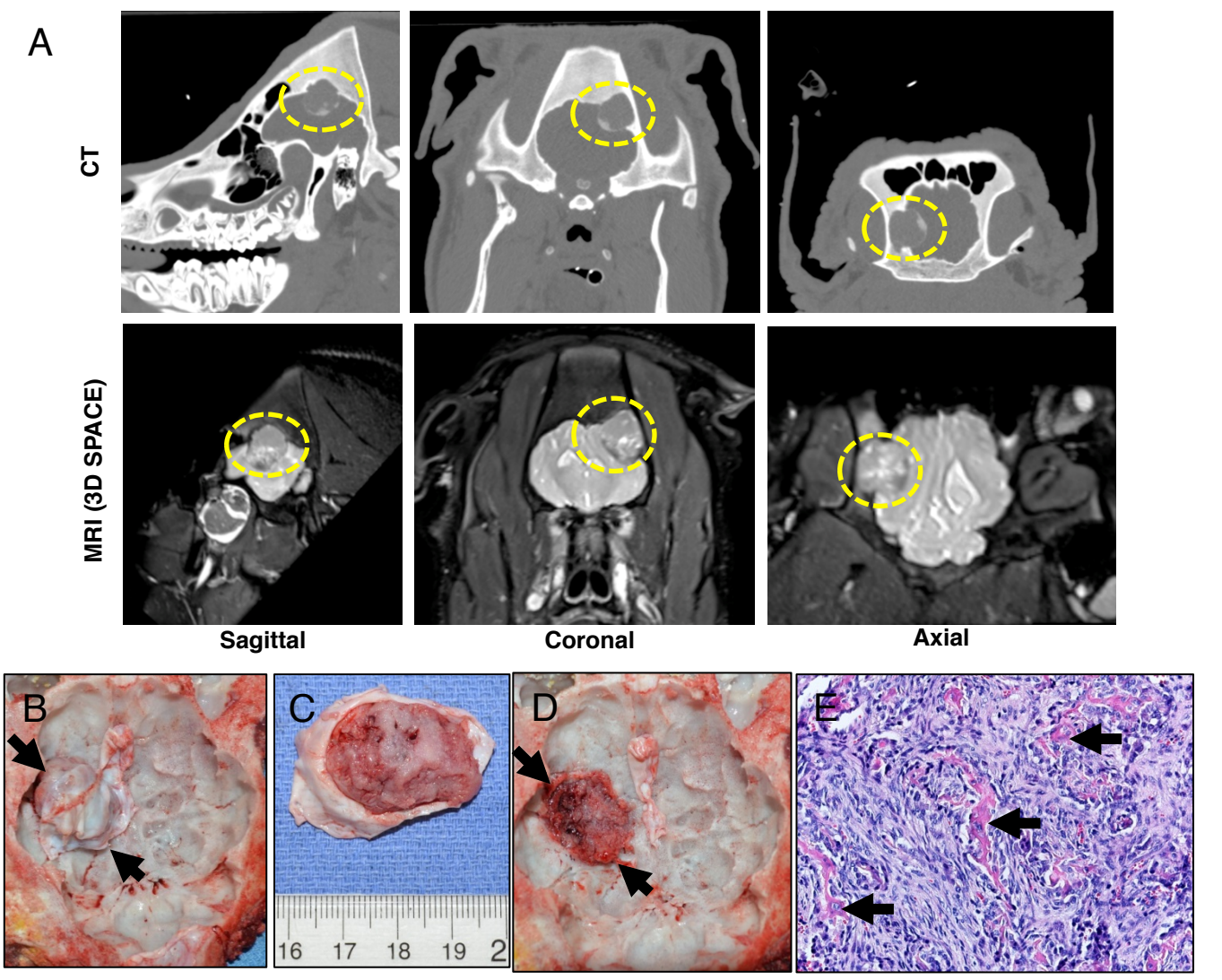

Figure S4: Osteogenic tumor in a *TP53*$^{R167H/R167H}$ pig (Case 5). A) In-vivo imaging with computed tomography (CT) and magnetic resonance (MR) non-invasively identified a 28 mm cranial tumor shown in sagittal, coronal and axial views. CT data revealed the tumor had a mean density (137 HU) below that of bone, and had invaded the calvarium/skull. MR imaging with a 3D SPACE sequence demonstrated the heterogeneous content of the tumor and compression of brain tissue. B) The tumor (arrows, left panel) was external to but attached to the dura. C,D) Removal of the tumor (C) revealed lysis and invasion of the tumor into the adjacent calvarium (arrows, D). E) The tumor was composed of spindle to round cells that produced irregular trabeculae of osteoid (arrows), 200x.

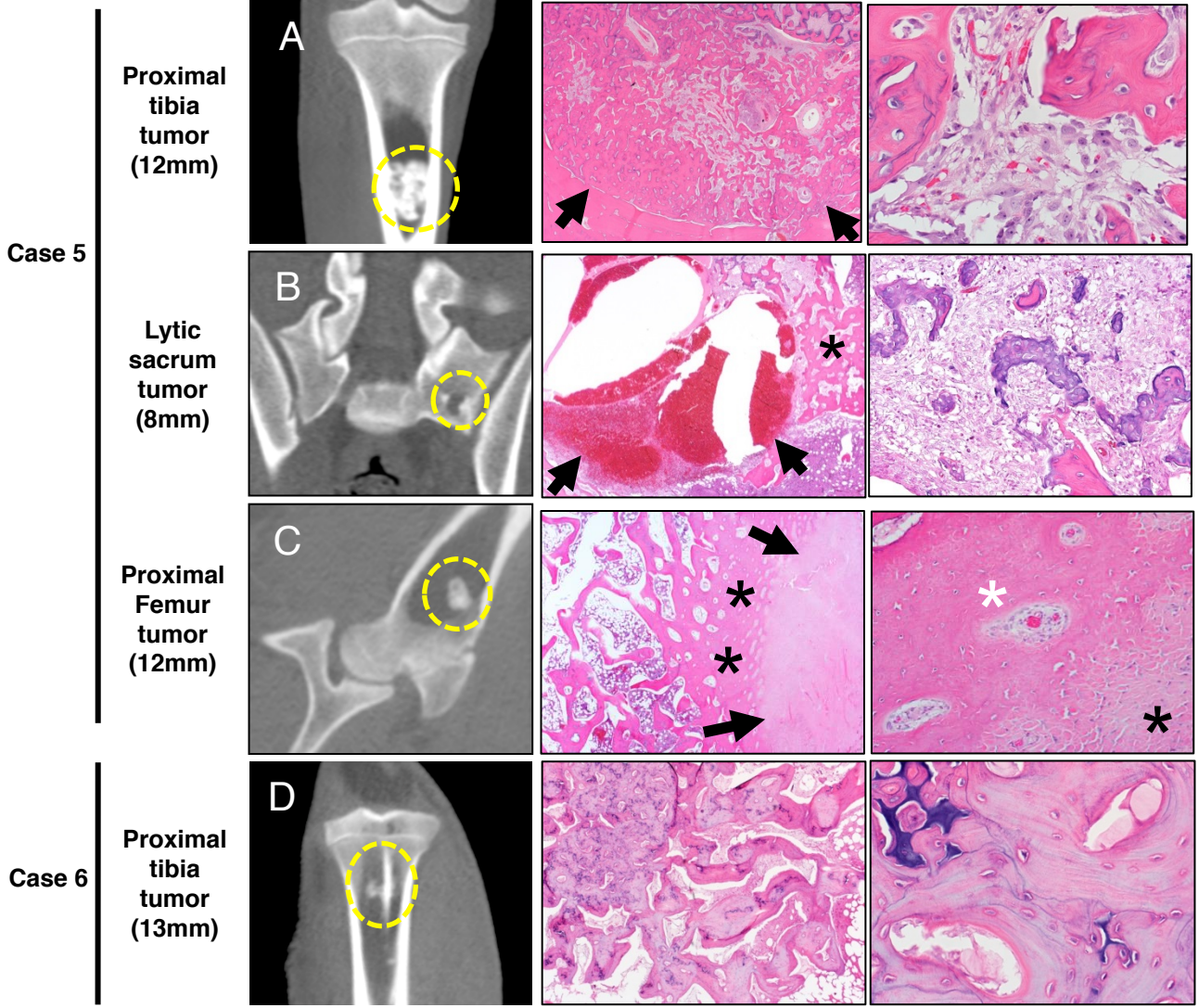

Figure S5. Examples of osteogenic tumors in the *TP53*$^{R167H/R167H}$ pigs. A) Proximal tibia tumor (arrows, 20x) was composed of coalescing bone trabeculae that effaced most of bone marrow to edges of cortex . Inter-trabecular bone marrow had plump spindle cells (right, 400x) with 1-2 nucleoli. 20x and 400x. B) Sacrum tumor (arrows) was composed of large blood filled spaces that were partially surrounded by dense bone (asterisk, 20x) and in other areas by loose connective tissue (right, 200x) with cartilaginous/osteoid production. C) The tumor (arrows) was surrounded by a rim of hyperdense osteosclerosis (asterisks, middle, 20x) and composed of a low cellularity non-mineralized zone (black asterisk, right, 200x) that merged into a mineralized zone (white asterisk, right) and eventual sclerotic bone (top left of right image). D) Proximal tibial tumor was composed of focal increase of coalescing trabeculae (middle, 20x) of osteoid and lamellar bone sometimes with central cartilage-like cores (deep blue color, right, 400x) and lined by scattered loose connective tissue with uncommon osteoblasts.

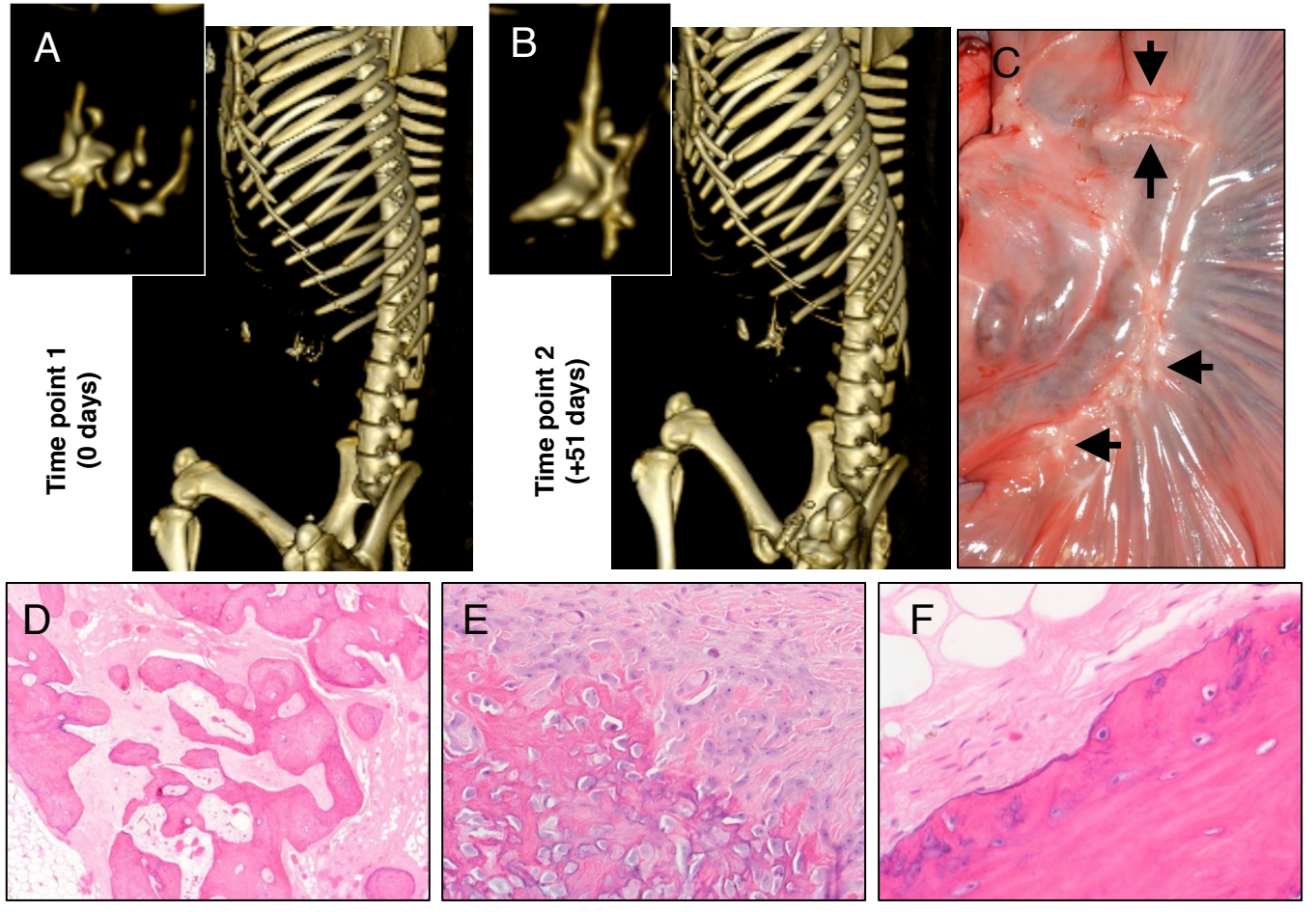

Figure S6. Mesenteric lesion in a *TP53*$^{R167H/R167H}$ pig (Case 6). A,B) Volumetric reconstruction of the skeletal system and mesenteric lesion from computed tomography data at time point 1 (A) and time point 2 (B) showing change in the structure of the lesion over the 7 week time period between data points. C) The mesentery had locally extensive ossification (arrows, C). D-F) The bony tissue (D, 40x) ranged from plump spindle cells with progressive osteoid/mineralization (E, 400x) to mature bone with a thin with rim of fibrous tissue (F, 400x).

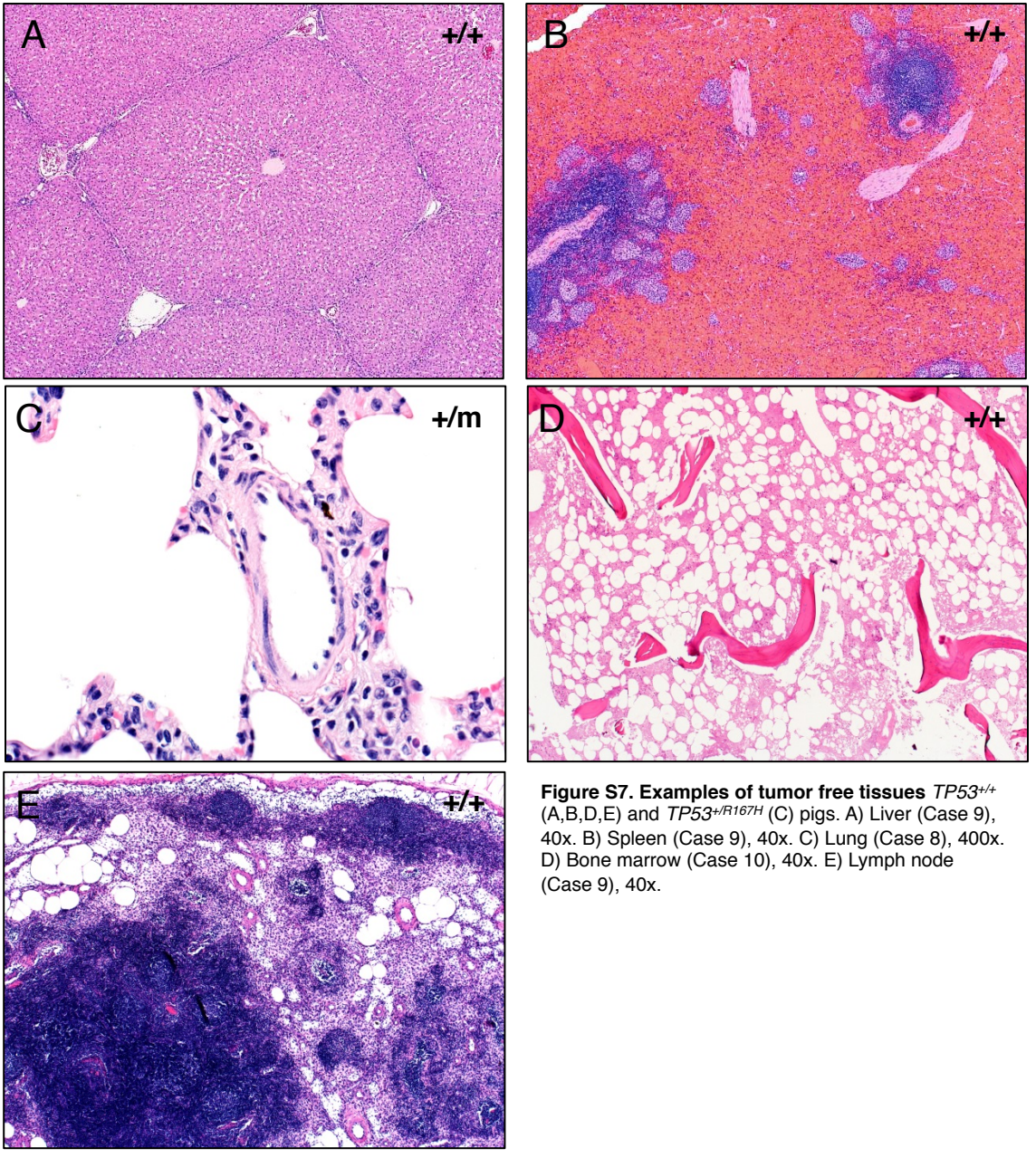

Figure S7. Examples of tumor free tissues *TP53*$^{+/+}$ (A,B,D,E) and *TP53*$^{+/R167H}$ (C) pigs. A) Liver (Case 9), 40x. B) Spleen (Case 9), 40x. C) Lung (Case 8), 400x. D) Bone marrow (Case 10), 40x. E) Lymph node (Case 9), 40x.

Supplemental Table 1. Case numbers, age, clinical and pathological features of necropsied pigs.

Case	Age	Clinical signs	Lesions
1 *TP53*$^{R167H/R167H}$	2 hours	Perinatal death	Liver: Hepatocellular atypia
2 *TP53*$^{R167H/R167H}$	6.75 months	Sudden death	Lymphoma Tumor lysis syndrome
3 *TP53*$^{R167H/R167H}$	7.75 months	Loss of body condition, weight loss	Lymphoma
4 *TP53*$^{R167H/R167H}$	10.75 months	Progressive lethargy, anorexia, weight loss, and reduced mobility in the 3-4 weeks prior to necropsy	Lymphoma
5 *TP53*$^{R167H/R167H}$	12.5 months	Listless and hyporesponsive to external stimuli at time of euthanasia	Osteogenic tumors
6 *TP53*$^{R167H/R167H}$	15.25 months	None	Osteogenic tumors Renal tumor (Wilms tumor/Nephroblastoma)
7 *TP53*$^{+/R167H}$	7.75 months	None	None
8 *TP53*$^{+/R167H}$	18.25 months	None	None
9 *TP53*$^{+/+}$	7.75 months	None	None
10 *TP53*$^{+/+}$	14.5 months	None	None

Supplemental Table 2. Expected morphology and site of origin for selected bone tumors and tumor-like conditions in humans.

Type	Morphology	Site(s) of origin
Osteosarcoma (59, 79-81)	Mesenchymal cells producing osteoid/bone often subdivided into osteoblastic, chondroblastic and fibroblastic subtypes	Metaphysis of long bones (esp. distal femur and proximal tibia and humerus); skull, jaw and pelvis
Osteoid osteoma (82-84)	Immature bone with increased vascularity and nerves; often with a rim of sclerotic bone	Long bones especially of lower extremity (e.g. femur); also reported in foot and spine; preference for diaphysis / metaphysis regions of long bones often near cortex
Giant cell tumor of bone (85)	Sheets of mononuclear osteoblastic cells admixed with numerous, prominent multinucleate cells (osteoclasts)	Most common in epiphysis/metaphysis of long bones (e.g. distal femur, proximal tibia, and distal radius) and also in sacrum/spine; rare in hands, feet, patella, talus
Aneurysmal bone cyst (ABC) (86, 87)	Lakes of bloods (not lined by endothelial cells) associated with proliferating fibroblasts, osteoclasts and reactive bone	Most common in long bones (~73%), also reported in pelvis, spine, foot, scapula, sacrum and ribs. 20% (2/10 cases) of ABCs in sacrum were associated with tumors
Heterotopic mesenteric ossification / myositis ossificans (88, 89)	Sclerosing mesenteritis with fat necrosis and eventual bone/osteoid formation	Bone formation in mesentery and/or serosa often as a sequela to traumatic injury or hemorrhage

Supplemental Table 3. PCR, RT-PCR, and Sequencing primers (all sequences 5' to 3')

pTP53seq 1F: CGCTCTCAATAATAGAGAACC

pTP53seq 2F: GAAATCATGCAGTGAATTTAAGT

pTP53seq 3F: CTAGGTCAACATAAAGGAGCG

pTP53seq 4F: TGAGCTGGGAGATGAGATGA

pTP53seq 5F: AGGGTGCTAGAAGATGAGATC

pTP53seq 6F: TGCAATGGAGGAGTCGCAG

pTP53seq 7F: CCTGGCAGCTATGATTTCCG

pTP53seq 8F: GTGCAGCTGTGGGTCAGC

pTP53seq 9F: CTCACTTGACCTGCCGCAG

pTP53seq 10F: GCTGGCTTTCCTCACTGC

pTP53seq 11F: GCTTGACTCTTGTAGTGCATA

pTP53seq 12F: GCGAGTTAAGAACTGGACTAG

pTP53seq 13F: TTCCCACTTCTAGCAACCCT

pTP53seq 6R: CTGCGACTCCTCCATTGCA

pTP53seq 7R: CGGAAATCATAGCTGCCAGG

pTP53 5'armF (EcoRV): gatcga*gatatc*GAGGTGTTTTCAGTGCCATTA

pTP53 5'armR (EcoRV): gatcga*gatatc*CAGCCAAGTGCTCGGTGG

pTP53 3'armF (BamHI): gatcga*ggatcc*CTAATCAGTATTTAGGCAGCG

pTP53 3'armRv2 (HindIII): gatcga*aagctt*GGTTGCAGAAGAGACTCCG

R167H-F: TGACCGAGGTGGTGAGGCACTGTCCCCACCATGAGCG

R167H-R: CGCTCATGGTGGGGACAGTGCCTCACCACCTCGGTCA

TP53-R167H-AAV-F (NotI): agctacat*gcggccgc*GCTGAGTTACTTCATCCTGAT

TP53-R167H-R (NotI): agctacat*gcggccgc*CAAAAGGATGGCTAGAGAAAC

Screen F (NeoR): AGACGTGCTACTTCCATTTGTCAC

pTP53 PCR-R1: TCAATCTCTCAAACCCGATAG

LDLR 5F: AGCCACAGCTCATCACTCC

LDLR-Exon5R1: AGCACTGGAACTCGTCAGG

P53oligoProbe-3: GTGAGGCACTGTCCCC

PGK-NeoF: CCAGTGTGCTGGAATTCGG

NeoR-R: CTGCAGAATTCGGCTTGTACT

pTP53 Southern probe 3F: GATGTGGCTCGGATCTGGT

pTP53 Southern Probe 3R: CCATGTTCCTCCCTGCTCC

PGK-F: GGCTGCTAAAGCGCATGCT

P53 Geno 4F: ACCCTGCCATCTCTGGCTA

P53NeoExc.Screen 3R: AGAGCGAACAGAAGGTCAGA

P21 CDKN1A F: CTCCCAGGGCAGGAAACG

P21 CDKN1A R: TTGTTTCCAGCAGGACAAGG

β-actin F: GAGAAGAGCTACGAGCTGCC

β-actin R: AGGTAGTTTCGTGGATGCCG

H-RAS-G12V F: GCATCCCCTACATCGAGA

H-RAS-G12V R: TACTTCTGCCTGCTGGGG

Italicized letters indicate restriction enzyme sequences for cloning. Underlined letters indicate the R167H codon.

Supplemental References

59. Luetke, A., Meyers, P.A., Lewis, I., and Juergens, H. 2013. Osteosarcoma treatment - Where do we stand? A state of the art review. *Cancer treatment reviews*.

79. Klein, M.J., and Siegal, G.P. 2006. Osteosarcoma: anatomic and histologic variants. *American journal of clinical pathology* 125:555-581.

80. Kirby, E.J., Zhou, H.H., and Morales, L., Jr. 2011. Primary pediatric osteosarcoma of the skull. *The Journal of craniofacial surgery* 22:2399-2405.

81. Goes, M. 1952. Knochenwachstum und osteogens sarcom. *Strahlentherapie* 89:194-210.

82. Chotel, F., Franck, F., Solla, F., Dijoud, F., Kohler, R., Berard, J., and Abelin Genevois, K. 2012. Osteoid osteoma transformation into osteoblastoma: fact or fiction? *Orthopaedics & traumatology, surgery & research : OTSR* 98:S98-104.

83. Jaffe, H.L. 1935. Osteoid osteoma: a benign osteoblastic tumor composed of osteoid and atypical bone. *Archives of Surgery* 31:709-728.

84. Kitsoulis, P., Mantellos, G., and Vlychou, M. 2006. Osteoid osteoma. *Acta orthopaedica Belgica* 72:119-125.

85. Raskin, K.A., Schwab, J.H., Mankin, H.J., Springfield, D.S., and Hornicek, F.J. 2013. Giant cell tumor of bone. *The Journal of the American Academy of Orthopaedic Surgeons* 21:118-126.

86. Brastianos, P., Gokaslan, Z., and McCarthy, E.F. 2009. Aneurysmal bone cysts of the sacrum: a report of ten cases and review of the literature. *The Iowa orthopaedic journal* 29:74-78.

87. Mankin, H.J., Hornicek, F.J., Ortiz-Cruz, E., Villafuerte, J., and Gebhardt, M.C. 2005. Aneurysmal bone cyst: a review of 150 patients. *Journal of clinical oncology : official journal of the American Society of Clinical Oncology* 23:6756-6762.

88. Ioannidis, O., Sekouli, A., Paraskevas, G., Kotronis, A., Chatzopoulos, S., Papadimitriou, N., Konstantara, A., Makrantonakis, A., and Kakoutis, E. 2012. Intra-abdominal heterotopic ossification of the peritoneum following traumatic splenic rupture. *Journal of research in medical sciences : the official journal of Isfahan University of Medical Sciences* 17:92-95.

89. Patel, R.M., Weiss, S.W., and Folpe, A.L. 2006. Heterotopic mesenteric ossification: a distinctive pseudosarcoma commonly associated with intestinal obstruction. *The American journal of surgical pathology* 30:119-122.